Modulated Model Based Predictive Control with Switcher of Redundant States for a Three-Phase Cascade H-Bridge Multilevel STATCOM

Leonardo Comparatore, Jorge Rodas and Raúl Gregor
Laboratory of Power and Control Systems
Universidad Nacional de Asunción
Luque, Paraguay

Marco Rivera
Department of Electrical Engineering
Universidad de Talca
Curicó, Chile

***Abstract*—Due to problems caused by variable switching frequency a modulated model based predictive control was proposed for different topologies and their applications. However, for cascade H-bridge multilevel converters, there is another problem, the imbalance in the *dc*-link voltages. This paper proposes extend the modulated model based predictive control to a cascade H-bridge 7-level STATCOM, further including a switcher of redundant states to solve the imbalance voltage issue. Simulation results show improvements in terms of mean squared error, total harmonic distortion and balance voltages in the *dc*-links.**

***Index Terms*—Cascade H-bridge converter, fixed switching frequency, predictive control, switcher of redundant states.**

NOMENCLATURE

CHB	Cascade H-bridge.
MBPC	Model based predictive control.
MSE	Mean squared error.
PCC	Point of common coupling.
PQ	Power quality.
STATCOM	Static synchronous compensator.
THD	Total harmonic distortion.

I. INTRODUCTION

Power quality in utility grids have been affected by the problems caused by the widespread use of modern power electronic equipments and energy conversion units, mainly in the industrial area [1]. Reduce high-level harmonic distortion and reactive power balance or power factor correction are the main issues in the field of power efficiency and PQ. STATCOM is considered one of the core means to provide reliable distribution PQ [2], mitigate disturbances and improve the PQ in electrical systems [1]. Among all STATCOM topologies the CHB multilevel converter-based has gained increasing attention of the research community due to its modularity, low harmonic distortion and good scalability in medium-voltage, high-power applications [3], [4].

Several control strategies have been applied to CHB multilevel converter-based STATCOM, in order to solve PQ problems, a recent review is presented in [5]. MBPC, in particular, is a well-established control technique and one of the most relevant in the field of power converters and drives [6]. The main advantages of MBPC are the simple design based on prediction model and cost function, no modulation stage, easy inclusion of nonlinearities and requirements and constraints. However, in power electronic converters, due to the nonlinear operation of the semiconductor devices, only a finite number of states are allowed. The application of MBPC is simplified by this feature, because a lower computational cost is required [6]. Nevertheless, due to the finite number of possible states, the absence of modulator becomes a disadvantage. This causes, mainly, a wrong references variables tracking, and consequently, intermediate control actions can not be computed. Moreover, variable switching frequency operation is obtained, due to that MBPC not follow a given switching pattern, neither has a control of which control action was applied previously. All the aforementioned drawbacks generates different stresses and active power losses on the power semiconductor devices and bad performance of the system in terms of PQ and/or output waveforms [7]-[14].

The various drawbacks of the MBPC can be solved including the objectives in the cost function by a sub-function multiplied by a weighting factor. However, the heuristic design of weighting factors is considered another disadvantage [6].

In this context, the purpose of this paper is twofold. First, we extend the modulated MBPC presented in [7]-[10]. to a CHB 7-level STATCOM. Second, we obtain a naturally *dc*-link balance with the inclusion of a switcher of redundant states.

II. THREE-PHASE CHB MULTILEVEL STATCOM

Fig. 1 shows the three-phase 7-level CHB converter-based STATCOM coupled to the power grid and the load through a shunt power filter (L_f-R_f), connected in the PCC. The STATCOM is composed by three H-bridge cells ($n_c = 3$ number of cells) per phase with an independent *dc*-link for each cell. All *dc*-link buses have the same voltage v_{dc} and the same capacitance C_{dc} values. Each cell contains four switching devices which are activated with digital signals $s\phi_{ij}$, being ϕ the corresponding phase (a, b or c), i the cell number (1, 2 or 3) and j the switching device (1, 2, 3 or 4). With the purpose of avoiding a short-circuit in the *dc*-link, the signals $s\phi_{i1}$ and $s\phi_{i3}$ are complementary to $s\phi_{i2}$ and $s\phi_{i4}$ respectively. Then, to adjust the output voltage v_c^{ϕ}, only

978-1-5090-5326-1/17/$31.00 ©2017 IEEE

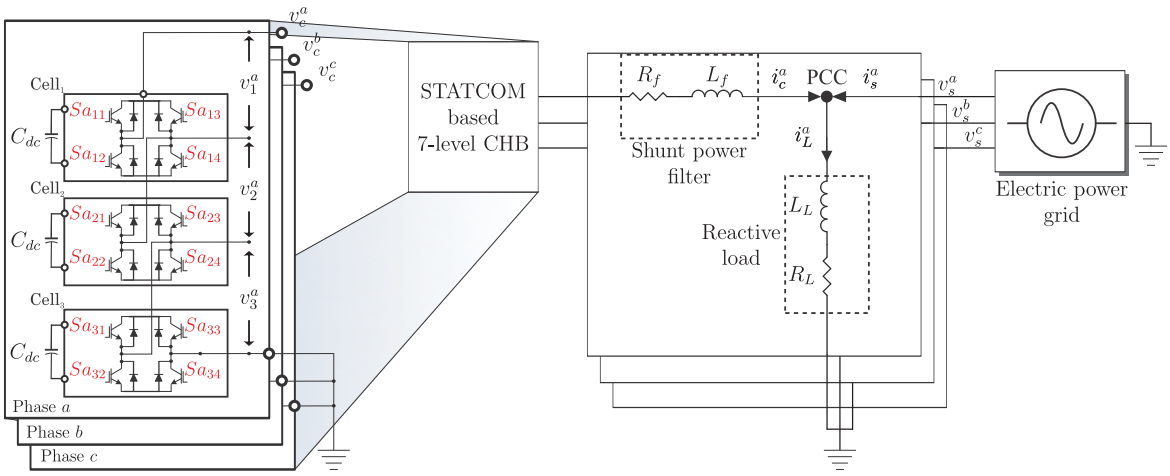

Fig. 1. Three-phase 7-level CHB converter-based STATCOM system connection.

$2n_c = 6$ signals are needed, with a total of $\varepsilon = 2^{2n_c} = 64$ possible switching states. Furthermore, each switching state corresponds to a switching function $F_s^\phi = \sum_{i=1}^{n_c} F_i^\phi$, where F_i^ϕ is the switching function for the cell i, whose possible values are shown in Table I.

TABLE I
SWITCHING FUNCTIONS FOR THE CELL "i"

$s\phi_{i1}$	$s\phi_{i3}$	$s\phi_{i2}$	$s\phi_{i4}$	F_i^ϕ
1	0	0	1	+1
1	1	0	0	0
0	0	1	1	0
0	1	1	0	−1

The possible values of F_s^ϕ are -3,-2, -1, 0, 1, 2 and 3, which are the seven levels of the STATCOM. As will be seen later, there are switching states ($\eta \in \{1, 2, \ldots, \varepsilon\}$) that produce the same value of F_s^ϕ. Then, the output voltage can be synthesized as a function of v_{dc} and F_s^ϕ, as:

$$v_c^\phi = F_s^\phi v_{dc} \tag{1}$$

Using Kirchhoff's circuit law, the continuous time-domain model of the CHB converter-based STATCOM is:

$$\frac{\mathrm{d}i_c^\phi}{\mathrm{d}t} = \frac{v_s^\phi}{L_f} - \frac{R_f}{L_f} i_c^\phi - \frac{v_c^\phi}{L_f} \tag{2}$$

where i_c^ϕ is the current injected by the CHB converter-based STATCOM and v_s^ϕ is the grid voltage.

The discrete time-domain model is obtained by using the forward-Euler discretization method:

$$i_c^\phi(k+1) = \left\{1 - \frac{R_f T_s}{L_f}\right\} i_c^\phi(k) + \frac{T_s}{L_f}\left\{v_s^\phi(k) - v_c^\phi(k)\right\} \tag{3}$$

where T_s is the sampling time, k identifies the actual discrete-time sample and $i_c^\phi(k+1)$ are the predictions of the STATCOM phase currents made at sample k.

III. MODULATED MODEL BASED PREDICTIVE CONTROL WITH SWITCHER OF REDUNDANT STATES

A. Classical MBPC

Classical MBPC methods use the mathematical model represented by (3), to have an accurate prediction of the behavior of the controlled variables, where the prediction is carried out for each possible switching state. Next, an optimization process uses this information to evaluate a cost function for each prediction to provide the control action that minimizes such cost function. Then, the control action selected is applied in the next sampling time during the whole switching period. The cost function is defined as a quadratic measure of the predicted error represented as follows:

$$g^\phi = \| ei_c^\phi(k+1) \|^2 = \| i_c^{\phi^*}(k+1) - i_c^\phi(k+1) \|^2 \tag{4}$$

where the superscript (*) indicates a reference variable.

The optimization process is described in Algorithm 1 and the block diagram is shown in Fig. 2(a).

Algorithm 1 Optimization algorithm of the classic MBPC

1. Initialize $g_{opt}^a := \infty, g_{opt}^b := \infty, g_{opt}^c := \infty, \eta := 0$
2. Compute $i_c^{a^*}(k+1)$, $i_c^{b^*}(k+1)$ and $i_c^{c^*}(k+1)$
3. **while** $\eta \leq \varepsilon$ **do**
4. Compute $i_c^a(k+1)$, $i_c^b(k+1)$ and $i_c^c(k+1)$
5. Compute $ei_c^a(k+1)$, $ei_c^b(k+1)$ and $ei_c^c(k+1)$
6. Compute g^a, g^b and g^c
7. **if** $g^a < g_{opt}^a$ **then**
8. $g_{opt}^a \leftarrow g^a, \quad F_{s,opt}^a \leftarrow F_{s,\eta}^a$
9. **end if**
10. **if** $g^b < g_{opt}^b$ **then**
11. $g_{opt}^b \leftarrow g^b, \quad F_{s,opt}^b \leftarrow F_{s,\eta}^b$
12. **end if**
13. **if** $g^c < g_{opt}^c$ **then**
14. $g_{opt}^c \leftarrow g^c, \quad F_{s,opt}^c \leftarrow F_{s,\eta}^c$
15. **end if**
16. $\eta := \eta + 1$
17. **end while**

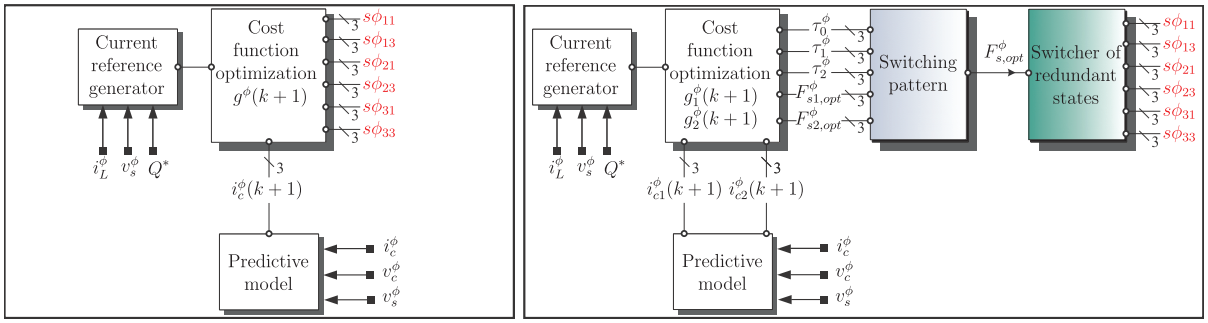

Fig. 2. Block diagram for: (a) the classical MBPC, (b) the proposed modulated MBPC with switcher of redundant states.

B. Proposed modulated MBPC

The main difference between the proposed method and the classical MBPC, is that the proposed method proceeds as space vector modulation. In space vector modulation, each sector is defined by two adjacent vectors (and one null vector), nonetheless, in this work, the "sectors" are defined by two consecutive active (or no-null) level and one null. The two optimum levels are chosen by an optimization process that evaluates the cost functions defined by (5) separately for each prediction and are applied during specified times, being their duty cycles inversely proportional to the respective cost functions. Next, all redundant states for the optimum levels are applied during their turn-on times, respectively. The block diagram of the proposed method is shown in Fig. 2(b), where the switching pattern and switcher of redundant states blocks are highlight.

C. Current reference generator

The instantaneous active and reactive power references are obtained from the well-known Clarke's transformation approach in $\alpha-\beta$ reference frame by using the following transformation matrix:

$$\mathbf{T}=\sqrt{\frac{2}{3}}\begin{bmatrix}1 & -\frac{1}{2} & -\frac{1}{2}\\ 0 & \frac{\sqrt{3}}{2} & -\frac{\sqrt{3}}{2}\\ \frac{1}{\sqrt{2}} & \frac{1}{\sqrt{2}} & \frac{1}{\sqrt{2}}\end{bmatrix} \tag{5}$$

Applying (5), the $\alpha-\beta$ current references at the AC side of the STATCOM are obtained as follows [15]-[17]:

$$\begin{bmatrix} i_{c\alpha}^* \\ i_{c\beta}^* \end{bmatrix}=\frac{1}{(v_{s\alpha})^2+(v_{s\beta})^2}\begin{bmatrix} v_{s\alpha} & v_{s\beta} \\ v_{s\beta} & -v_{s\alpha}\end{bmatrix}\begin{bmatrix} P_c^* \\ Q_c^*\end{bmatrix} \tag{6}$$

where the P_c^* and Q_c^* are the instantaneous active and reactive power references, respectively. In order to allow an unitary power factor at the grid side and considering which ideally the STATCOM do not absorb any active power, the instantaneous power references can be written as:

$$P_c^*=0 \tag{7}$$

$$Q_c^*=-Q_L=v_{s\alpha}i_{L\beta}-v_{s\beta}i_{L\alpha} \tag{8}$$

being Q_L the instantaneous reactive load power to be compensate by the CHB converter-based STATCOM system. Next, the STATCOM phase currents references used in the optimization process are:

$$[i_c^{a^*} \quad i_c^{b^*} \quad i_c^{c^*}]'=\mathbf{T}^{-1}[i_{c\alpha}^* \quad i_{c\beta}^* \quad 0]' \tag{9}$$

where the superscript ($'$) indicates the transposed matrix.

D. Cost function and duty cycles

The new cost function (for each phase ϕ) for the proposed method is defined as the weighted sum of the cost functions g_1^{ϕ} and g_2^{ϕ}, whose respective weighting factors are the duty cycles τ_1^{ϕ} and τ_2^{ϕ}, for two active levels, respectively, as:

$$g^{\phi}=\tau_1^{\phi}g_1^{\phi}+\tau_2^{\phi}g_2^{\phi} \tag{10}$$

where $g_1^{\phi}=\| \, ei_{c\,1}^{\phi}(k+1) \, \|^2$ and $g_2^{\phi}=\| \, ei_{c\,2}^{\phi}(k+1) \, \|^2$, defined as (5) for each predicted error.

The level that generates the lowest value of the cost function must be applied higher time, i.e., the duty cycle must be inversely proportional to the cost function. The duty cycles for the two active levels and one null are calculated by solving:

$$\begin{aligned}\tau_0^{\phi}&=K^{\phi}/g_0^{\phi}\\ \tau_1^{\phi}&=K^{\phi}/g_1^{\phi}\\ \tau_2^{\phi}&=K^{\phi}/g_2^{\phi}\\ \tau_0^{\phi}+\tau_1^{\phi}+\tau_2^{\phi}&=1\end{aligned} \tag{11}$$

where τ_0^{ϕ} correspond to the duty cycle of a null level which is evaluated only one time and K^{ϕ} is the constant of proportionality.

The expressions of the duty cycles for each level are given solving (11) for K^{ϕ} as:

$$\begin{aligned}\tau_0^{\phi}&=g_1^{\phi}g_2^{\phi}/\left(g_0^{\phi}g_1^{\phi}+g_1^{\phi}g_2^{\phi}+g_0^{\phi}g_2^{\phi}\right)\\ \tau_1^{\phi}&=g_0^{\phi}g_2^{\phi}/\left(g_0^{\phi}g_1^{\phi}+g_1^{\phi}g_2^{\phi}+g_0^{\phi}g_2^{\phi}\right)\\ \tau_2^{\phi}&=g_0^{\phi}g_1^{\phi}/\left(g_0^{\phi}g_1^{\phi}+g_1^{\phi}g_2^{\phi}+g_0^{\phi}g_2^{\phi}\right)\end{aligned} \tag{12}$$

being the turn-on times (T_0^{ϕ}, T_1^{ϕ} and T_2^{ϕ}) the products of multiplying the duty cycles (τ_0^{ϕ}, τ_1^{ϕ} and τ_2^{ϕ}) by the sampling time, respectively.

E. Switching pattern

At the end of the optimization process, the two optimum active levels ($F^{\phi}_{s1,opt}$ and $F^{\phi}_{s2,opt}$) and the one null level are applied during their respective turn-on times using the switching pattern procedure that is shown in Fig. 3, similar to [18], [19].

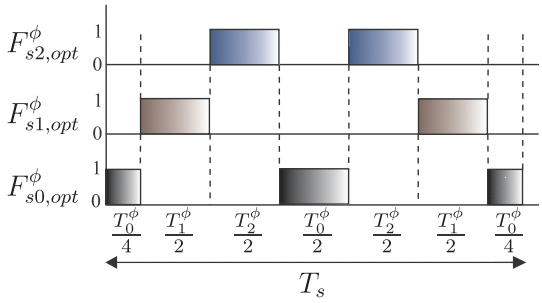

Fig. 3. Switching pattern for the optimal levels.

F. Switcher of redundant states

All redundant states for each optimal level are sequentially applied during a turn-on time (T^{ϕ}_i), with a duty cycle given by:

$$\tau^{\phi}_i = \frac{T^{\phi}_i}{r} \tag{13}$$

being r the amounts of redundant states for each level, as is shown in Table II.

TABLE II
AMOUNTS OF REDUNDANT STATES FOR EACH LEVEL

Level ($\times v_{dc}$)	-3	-2	-1	0	1	2	3
Redundant states (r)	1	6	15	20	15	6	1

To simplify the algorithm, is selected $r = 20$ for all levels, thus, the states of the levels with fewer amount of redundant states are reapplied until to complete the respective turn-on time.

For example, in case the levels 1 and 2 are selected, redundant states for levels 0, 1 and 2 are applied for a total time T^{ϕ}_0, T^{ϕ}_1 and T^{ϕ}_2, respectively, (for each phase ϕ), until completing a sampling period.

G. Optimization process

The optimization process consist in to compute, the predictions, the predicted errors, the cost functions and the duty cycles over all possible sectors (ϱ). Since there are 6 active levels (44 active switching states) and one null level (20 null switching states) for the case study, the computation is performed $\varrho = 6$ times. Once the optimum consecutive active levels have been obtained, their respective turn-on times are calculated. At the end of the optimization process, the two optimum active levels ($F_{s1,opt}$ and $F_{s2,opt}$) and the null level are applied during their respective turn-on times using the switching pattern procedure. The optimization process (for each phase ϕ) is illustrated in Algorithm 2.

Algorithm 2 Optimization algorithm of the proposed method

1. Initialize $g^{\phi}_{opt} := \infty, \eta := 0$
2. Compute $i^{*}_c(k+1)$
3. Compute $i^{\phi}_{c\,0}(k+1)$
4. Compute $ei^{\phi}_{c\,0}(k+1)$
5. Compute $g^{\phi}_0 = g^{\phi}_0(k+1)$
6. **while** $\eta \leq \varrho$ **do**
7. Compute $i^{\phi}_{c\,1}(k+1)$ and $i^{\phi}_{c\,2}(k+1)$
8. Compute $ei^{\phi}_{c\,1}(k+1)$ and $ei^{\phi}_{c\,2}(k+1)$
9. Compute $g^{\phi}_1 = g^{\phi}_1(k+1)$ and $g^{\phi}_2 = g^{\phi}_2(k+1)$
10. Compute τ^{ϕ}_0, τ^{ϕ}_1 and τ^{ϕ}_2
11. Compute $g^{\phi} = \tau^{\phi}_1 g^{\phi}_1 + \tau^{\phi}_2 g^{\phi}_2$
12. **if** $g^{\phi} < g^{\phi}_{opt}$ **then**
13. $g^{\phi}_{opt} \leftarrow g^{\phi}$
14. Compute T^{ϕ}_0, T^{ϕ}_1 and T^{ϕ}_2
15. $F^{\phi}_{s1,opt} \leftarrow F^{\phi}_{s1,\eta}, F^{\phi}_{s2,opt} \leftarrow F^{\phi}_{s2,\eta}$
9. **end if**
10. $\eta := \eta + 1$
11. **end while**

IV. SIMULATION RESULTS AND DISCUSSION

To validate the effectiveness of the proposed method, simulation results in Matlab/Simulink environment were carried out considering the electrical parameters shown in Table III. The performance of the proposed method is compared with the results obtained by a classical MBPC considering a 10 kHz of sampling frequency (to have a little more fair comparison, 30 kHz is used for classical MBPC). Numerical integration by means of the first-order forward-Euler method has been applied to compute the evolution of the controlled variables step by step in the time domain. The MSE between the reference and the actual value of the current [Eq. (14)], and the THD of the grid current [Eq. (15)] have been used as quality performance indices to compare quantitatively both controllers.

$$\text{MSE}(\Psi) = \sqrt{\frac{1}{N}\sum_{j=1}^{N}\Psi^2_j} \tag{14}$$

$$\text{THD} = \sqrt{\frac{1}{i^2_1}\sum_{i=2}^{N} i^2_i} \tag{15}$$

being Ψ the tracking current error, N the number of vector elements, i_1 the amplitude of the fundamental frequency of the analyzed current, and i_i the current harmonics.

Fig. 4 shows the effect of the instantaneous reactive power compensation, showing a fast dynamic response during the transient. The big spikes are consequence of the application of the null vector in the switching pattern. Moreover, Fig. 5, shows the current tracking (phase a) dynamic performance for a step change of the reactive power reference; considering the interval 0.02 s to 0.1 s, the proposed method reduce the MSE parameter from 0.3352 A to 0.3110 A (about 7 %). Fig. 6

TABLE III
PARAMETERS DESCRIPTION

PARAMETER	SYMBOL	VALUE	UNIT
	Electric power grid		
Grid frequency	f_e	50	Hz
Grid voltage	v_s	310.2	V
	7-Level CHB STATCOM		
Filter resistance	R_f	0.09	Ω
Filter inductance	L_f	3	mH
DC-link voltage	v_{dc}	154	V
	Load parameters		
Load resistance	R_L	23.2	Ω
Load inductance	L_L	55	mH
	Predictive control parameters		
Sampling time	T_s	40	μs
Simulation step	–	1	μs

shows the THD behavior of the grid current (phase a). It can be observed from the simulation results that the THD parameter is reduced from 5.17 % to 4.39 %. As shown in Fig. 7 (upper) a more sinusoidal output voltage v_c^a is obtained with respect to the output voltage than in Fig. 7 (bottom) due to the switching pattern procedure. On the other hand, the voltage output switching pattern is shown in Fig. 8 (upper). It is noted as the two optimum active levels and the one null applied to STATCOM during a sampling period exhibit the proposed sequence. Furthermore, a better performance is obtained in terms of voltage ripple and a simultaneous charge/discharge process on the capacitors, of the H-bridge cells corresponding to phase a, as the Fig. 9 shows. Similar results were obtained for b and c phases.

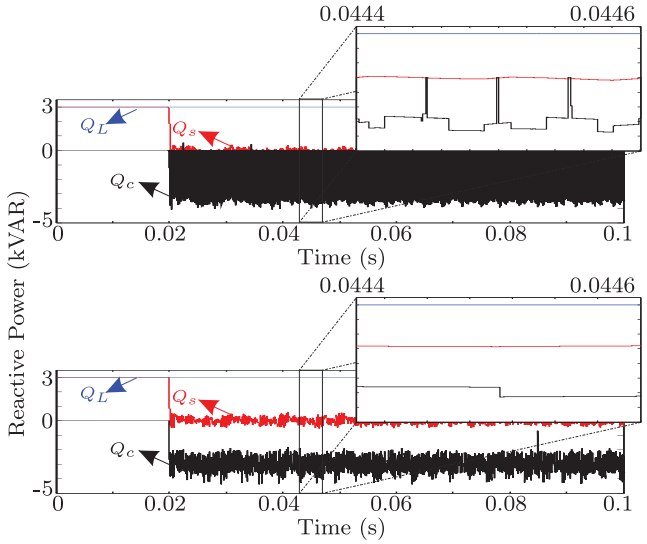

Fig. 4. Reactive power reference and compensation: (upper) proposed controller, (bottom) classical MBPC.

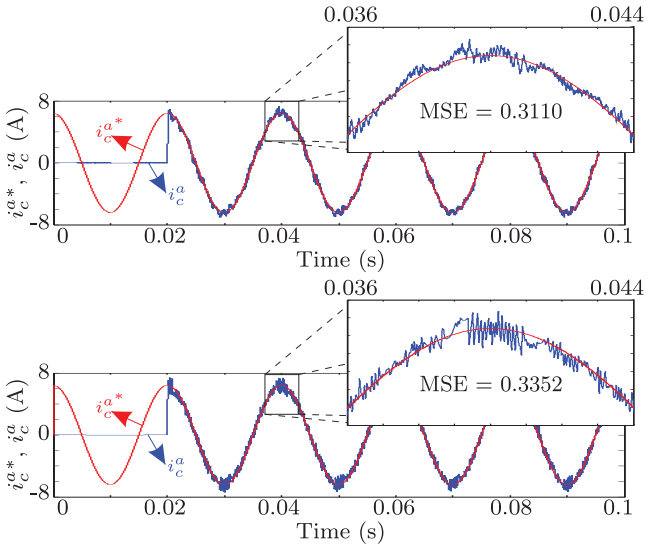

Fig. 5. Current tracking: (upper) proposed controller, (bottom) classical MBPC.

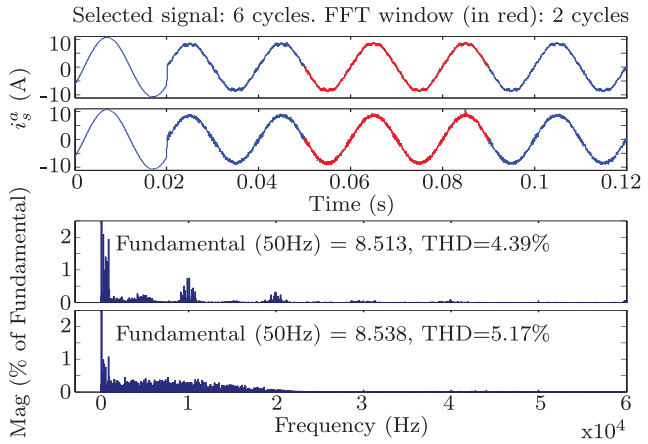

Fig. 6. THD of the grid current: (upper) proposed controller, (bottom) classical MBPC.

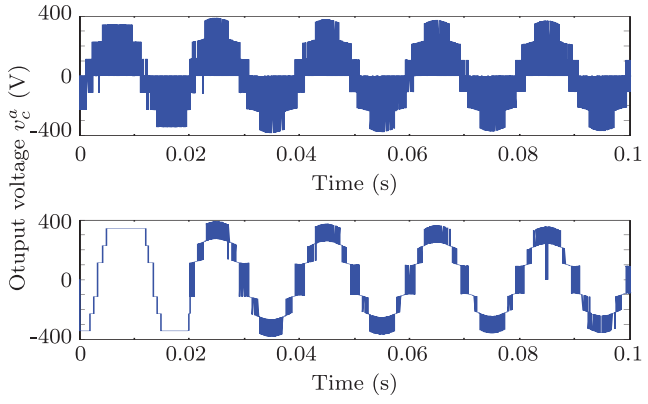

Fig. 7. Output voltage of the STATCOM: (upper) proposed controller, (bottom) classical MBPC.

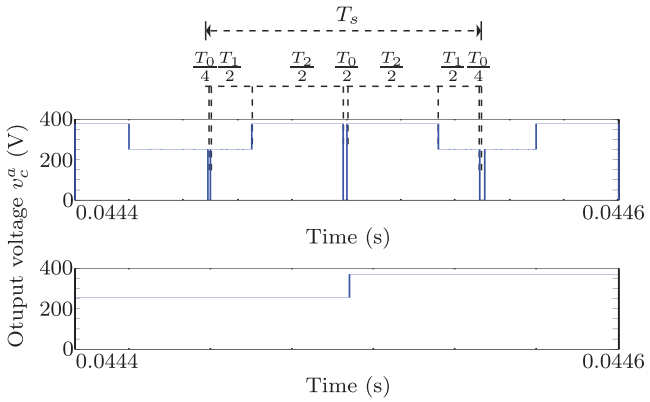

Fig. 8. Switching pattern of the output voltage: (upper) proposed controller, (bottom) classical MBPC.

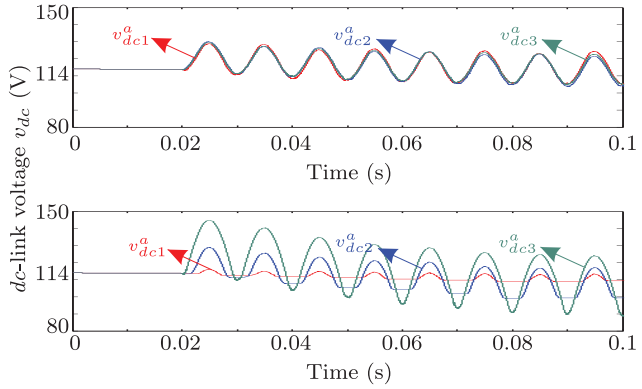

Fig. 9. Voltage evolution on the capacitors: (upper) proposed controller, (bottom) classical MBPC.

V. Conclusion

In this paper, a modulated MBPC with switcher of redundant states applied to the three-phase three-wire 7-level CHB STATCOM has been proposed. Simulation results confirm the capability of the proposed control technique to compensate the instantaneous reactive power and shows that it is possible to increase the performance in terms of MSE and THD, thanks to the operation at fixed switching frequency, compared with the results obtained by the classical MBPC. Reduction in the MSE parameter is about 7% and the improvement in the THD performance parameter is about 15.1% . A comparative simulation results performed with reference to the classical MBPC also show improvements relative to balance voltages in the *dc*-links, showing a simultaneous charge/discharge process.

Acknowledgment

The authors would like to thank to the Paraguayan Government for the economical support they provided through the CONACYT Grant 14-INV-096. This work was also made possible by the FONDECYT Regular Project N° 1160690.

References

[1] S. A. Kamran and J. Muñoz, "Study of a state-of-the art M-STATCOM," in *Proc. ICIT*, 2015, pp. 2733–2738.

[2] Y. Ma, L. Cao, X. Zhou, and Z. Gao, "The discussion on static synchronous compensator technology," in *Proc. ICMA*, 2016, pp. 106–111.

[3] C. D. Townsend, T. J. Summers, and R. E. Betz, "Phase-shifted carrier modulation techniques for cascaded H-bridge multilevel converters," *IEEE Trans. Ind. Electron.*, vol. 62, no. 11, pp. 6684–6696, 2015.

[4] Y. Yu, G. Konstantinou, B. Hredzak, and V. G. Agelidis, "Operation of cascaded H-bridge multilevel converters for large-scale photovoltaic power plants under bridge failures," *IEEE Trans. Ind. Electron.*, vol. 62, no. 11, pp. 7228–7236, 2015.

[5] J. Muñoz, J. Rohten, J. Espinoza, P. Melin, C. Baier, and M. Rivera, "Review of current control techniques for a cascaded H-bridge STATCOM," in *Proc. ICIT*, 2015, pp. 3085–3090.

[6] S. Kouro, M. A. Perez, J. Rodriguez, A. M. Llor, and H. A. Young, "Model predictive control: MPC's role in the evolution of power electronics," *IEEE Ind. Electron. Mag.*, vol. 9, no. 4, pp. 8–21, 2015.

[7] L. Tarisciotti, P. Zanchetta, A. Watson, J. C. Clare, M. Degano, and S. Bifaretti, "Modulated model predictive control for a three-phase active rectifier," *IEEE Trans. Ind. Electron.*, vol. 51, no. 2, pp. 1610–1620, 2015.

[8] M. Rivera, F. Morales, C. Baier, J. Muñoz, L. Tarisciotti, P. Zanchetta, and P. Wheeler, "A modulated model predictive control scheme for a two-level voltage source inverter," in *Proc. ICIT*, 2015, pp. 2224–2229.

[9] M. Vijayagopal, P. Zanchetta, L. Empringham, L. D. Lillo, L. Tarisciotti, and P. Wheeler, "Modulated model predictive current control for direct matrix converter with fixed switching frequency," in *Proc. EPE/ECCE*, 2015, pp. 1–10.

[10] L. Tarisciotti, P. Zanchetta, A. Watson, S. Bifaretti, and J. C. Clare, "Modulated model predictive control for a seven-level cascaded H-bridge back-to-back converter," *IEEE Trans. Ind. Electron.*, vol. 61, no. 10, pp. 5375–5383, 2014.

[11] M. Rivera, "A new predictive control scheme for a VSI with reduced common mode voltage operating at fixed switching frequency," in *Proc. POWERENG*, 2015, pp. 617–622.

[12] M. Vijayagopal, L. Empringham, L. de Lillo, L. Tarisciotti, P. Zanchetta, and P. Wheeler, "Current control and reactive power minimization of a direct matrix converter induction motor drive with modulated model predictive control," in *Proc. PRECEDE*, 2015, pp. 103–108.

[13] R. Rabbeni, L. Tarisciotti, A. Gaeta, A. Formentini, P. Zanchetta, M. Pucci, M. Degano, and M. Rivera, "Finite states modulated model predictive control for active power filtering systems," in *Proc. ECCE*, 2015, pp. 1556–1562.

[14] M. Tomlinson, T. Mouton, and R. Kennel, "Finite-control-set model predictive control with a fixed switching frequency vs. linear control for current control of a single-leg inverter," in *Proc. PRECEDE*, 2015, pp. 109–114.

[15] R. Gregor, L. Comparatore, A. Renault, J. Rodas, J. Pacher, S. Toledo, and M. Rivera, "A novel predictive-fixed switching frequency technique for a cascade H-bridge multilevel STATCOM," in *Proc. IECON*, 2016, pp. 3672–3677.

[16] L. Comparatore, R. Gregor, J. Rodas, J. Pacher, A. Renault, and M. Rivera, "Model based predictive current control for a three-phase cascade H-bridge multilevel STATCOM operating at fixed switching frequency," in *Proc. PEDG*, 2017, pp. 1–6.

[17] L. Comparatore, A. Renault, J. Pacher, R. Gregor, J. Rodas, and M. Rivera, "Model based predictive control with switcher of redundant vectors for a cascade H-bridge multilevel STATCOM," in *Proc. ANDESCON*, 2016, pp. 1–4.

[18] L. K. Haw, M. S. Dahidah, and H. A. Almurib, "A new reactive current reference algorithm for the STATCOM system based on cascaded multilevel inverters," *IEEE Trans. Power Electron.*, vol. 30, no. 7, pp. 3577–3588, 2015.

[19] Y. Neyshabouri, H. Iman-Eini, and M. Miranbeigi, "State feedback control strategy and voltage balancing scheme for a transformer-less static synchronous compensator based on cascaded H-bridge converter," *IET Power Electron.*, vol. 8, no. 6, pp. 906–917, 2015.